

# A wide-field spectroscopic survey of the cluster of galaxies Cl0024+1654

## II. A high-speed collision?\*

Oliver Czoske<sup>1,2</sup>, Ben Moore<sup>3</sup>, Jean-Paul Kneib<sup>1</sup>, and Geneviève Soucail<sup>1</sup>

<sup>1</sup> Observatoire Midi-Pyrénées, UMR5572, 14 Av. Edouard Belin, 31400 Toulouse, France

<sup>2</sup> Institute for Astronomy, University of Hawaii, 2680 Woodlawn Drive, Honolulu HI 96822, USA

<sup>3</sup> Department of Physics, Durham University, South Road, Durham, DH1 3LE, UK

Received too late, Accepted even later

**Abstract.** The mass distribution of the rich cluster of galaxies Cl0024+1654 has frequently been used to constrain the nature of dark matter yet a model consistent with all the observational data has been difficult to construct. In this paper we analyse the three-dimensional structure of this cluster using new spectroscopic information on  $\sim 300$  galaxies within a projected radius of  $3 h^{-1}$  Mpc. These data reveal an unusual foreground component of galaxies separated from the main cluster by  $3000 \text{ km s}^{-1}$ . We use numerical simulations to show that a high speed collision along the line of sight between Cl0024+1654 and a second cluster of slightly smaller mass can reproduce the observed peculiar redshift distribution. The collision dramatically alters the internal mass distribution of the bound remnants, creating constant density cores from initially cuspy dark matter profiles and scattering galaxies to large projected radii. Our results can reconcile the inferred mass profile from gravitational lensing with predictions from hierarchical structure formation models, while at the same time resolving the mass discrepancy that results from a comparison between lensing, velocity dispersion and X-ray studies.

**Key words.** galaxies: clusters: Cl0024+1654 – cosmology: observations – cosmology: large-scale structure of the Universe

### 1. Introduction

The nature of the ubiquitous dark matter remains one of the major mysteries in cosmology. The traditional view is that the dark matter is cold, i. e. non-relativistic at the decoupling epoch, and only subject to gravitational and weak interactions. Structure formation with this type of dark matter has been investigated extensively through numerical simulations over the past 25 years. High-resolution simulations of individual cold dark matter halos have shown that the mass distribution in CDM halos over a wide range of total masses, from dwarf galaxy to cluster scales, should follow a universal profile (Navarro et al. 1997, NFW); in particular, the mass distribution is found to have a central cusp with logarithmic slope of  $-1.5$  (Moore et al. 1998; Ghigna et al. 2000). Recent observational results, however, have challenged this simple picture.

The rich cluster of galaxies Cl0024+1654 at  $z = 0.395$  features a spectacular quintuple gravitational arc system of radius  $106 h^{-1} \text{ kpc}$  that has been used to reconstruct the projected central mass distribution (Kassiola et al. 1992; Smail et al. 1996; Tyson et al. 1998; Broadhurst et al. 2000). Constructing a mass model for this cluster that is consistent with all the observations has proved very difficult, however. The total projected mass enclosed within the arc radius is fairly well constrained and yields a value of about  $1.6 \times 10^{14} h^{-1} M_{\odot}$ . To reproduce this mass with an NFW type profile would require a cluster with characteristic velocity dispersion larger than  $2000 \text{ km s}^{-1}$  (Broadhurst et al. 2000; Shapiro & Iliev 2000). This is much higher than observed in this or indeed in any other cluster of galaxies. The mass reconstruction by Tyson et al. (1998), based on the detailed structure of the gravitationally lensed background spiral galaxy, shows a flat core in the projected central mass distribution with a core radius of  $35 h^{-1} \text{ kpc}$ . This apparent contradiction to the predictions of standard CDM simulations has prompted a number of authors to investigate alternatives to the classic CDM scenario, e. g. warm dark matter, self-interacting

Send offprint requests to: O. Czoske, e-mail: oczoske@ast.obs-mip.fr

\* Based on observations obtained with the Canada–France–Hawaii Telescope and the William–Herschel Telescope.

dark matter, etc. (Spergel & Steinhardt 2000; Hogan & Dalcanton 2000; Moore et al. 2000).

As more detailed observations of individual clusters of galaxies are compiled, combinations of X-ray imaging and spectroscopy, velocity dispersion measurements and lensing mass maps frequently reveal that clusters that were thought to be simple relaxed objects are actually more complex systems, frequently undergoing mergers or generally showing signs of substructure and deviations from dynamical equilibrium. Evidence for recent mergers or accretion is currently accumulating through CHANDRA observations in the form of merger shocks (e. g. Markevitch & Vikhlinin 2001; Markevitch et al. 2001) or cold fronts (Markevitch et al. 2000; Vikhlinin et al. 2001; Mazzotta et al. 2001). Mergers and substructure have also been invoked to explain the discrepancy between mass estimates from different methods that is observed in many clusters (Miralda-Escudé & Babul 1995; Wu et al. 1998).

Cl0024+1654 is an example of a cluster where the high mass inferred from the strong lensing mass reconstructions is at variance with the fairly low X-ray luminosity and temperature, that indicate a total mass for the cluster which is a factor 2 to 3 smaller than the lensing mass (Soucail et al. 2000). Both the galaxy distribution on the sky and the X-ray morphology are regular and by themselves compatible with a relaxed massive cluster, a notion which was further supported by the high galaxy velocity dispersion of  $\approx 1200 \text{ km s}^{-1}$  found in the redshift surveys of Dressler & Gunn (1992) and Dressler et al. (1999) (hereafter D99).

In Czoske et al. (2001, Paper I) we presented a new catalogue of 650 measured redshifts (including those from D99) in a wide field around Cl0024+1654. 300 galaxies in the catalogue have redshifts in the range  $0.37 < z < 0.42$ , i. e. are cluster members or lie in the immediate neighbourhood of the cluster, and the redshift distribution of these galaxies was found in Paper I to be distinctly bimodal. In the present paper we analyse the distribution of the galaxies in redshift/real space and present a merger scenario which is able to reconcile all the observations. Section 2 recalls the data used and describes the distribution of the redshifts, colours, and equivalent widths of important lines. In Section 3, we develop the merger scenario and use numerical simulations to show that it is possible to explain the peculiar three-dimensional distribution of the galaxies in Cl0024+1654. In Section 4 we show how the observed structure is able to explain and resolve the discrepancy of mass estimates of Cl0024+1654 derived from different observations. Finally, in Section 5 we summarize and conclude.

Throughout this paper we use a Hubble constant  $H_0 = 100 h^{-1} \text{ km s}^{-1} \text{ Mpc}^{-1}$  and assume an Einstein-de Sitter Universe with  $\Omega_M = 1$  and  $\Omega_\Lambda = 0$ .

## 2. The cluster environment

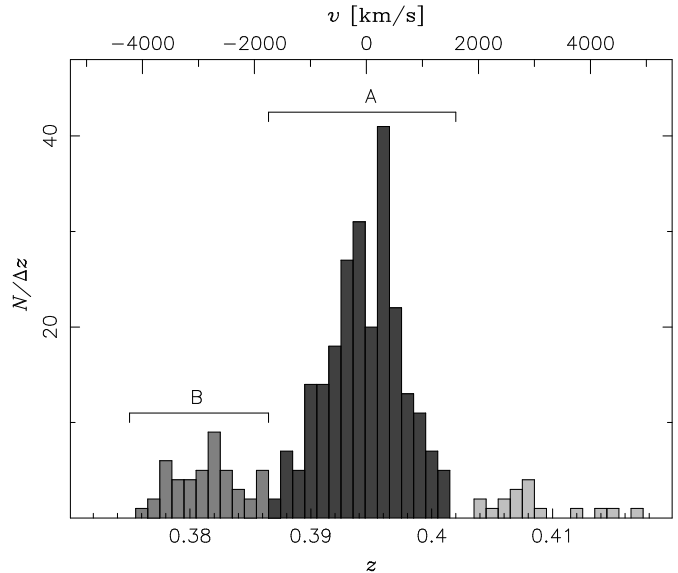


**Fig. 1.** Redshift histogram for 300 objects in the neighbourhood of Cl0024+1654 ( $0.37 < z < 0.42$ ). The attribution of galaxies to components A (dark grey) and B (light grey) was done by inspection of Fig. 2. Whereas the lower and upper redshift limits of components B and A respectively are fairly secure, the exact demarcation between the two components is arbitrary to some extent and was chosen at  $\Delta v = -1500 \text{ km s}^{-1}$  with respect to the central redshift of component A, Eq. (1)

### 2.1. The data

In Paper I we presented a new catalogue of photometric and spectroscopic data for 679 objects in a wide field of  $21 \times 25 \text{ arcmin}^2$  around Cl0024+1654. At the redshift of the cluster,  $z = 0.395$ , this corresponds to  $4 \times 4.8 h^{-2} \text{ Mpc}^2$  (the true survey field is delimited by an irregular polygon inscribed in this rectangle and covers  $16.8 h^{-2} \text{ Mpc}^2$ , see Fig. 5, or Fig. 7 in Paper I). The catalogue lists equatorial position, redshift,  $V$  magnitude,  $V - I$  colour, equivalent widths for  $[\text{O II}] \lambda 3727$ ,  $[\text{O III}] \lambda 5007$ ,  $\text{H}\alpha$  (where within the wavelength range),  $\text{H}\beta$  and  $\text{H}\delta$ , as well as the strength of the  $4000\text{\AA}$  break. Here we are only concerned with the 650 objects having measured redshifts, of which 581 were observed by us at CFHT and WHT, with the remaining 69 taken from Dressler et al. (1999). See Paper I for more technical details on the data used in this paper.

### 2.2. Redshift distribution

Fig. 1 shows a histogram of the 300 redshifts that lie in the range  $0.37 < z < 0.42$ . The redshift distribution of the cluster galaxies is clearly bimodal, showing two peaks at  $z = 0.381$  and  $z = 0.395$  respectively; these peaks contain 283 galaxies.

The larger peak at  $z = 0.395$  ( $0.387 < z < 0.402$ , hereafter referred to as component A) contains 237 galaxies, is fairly regular and resembles a Gaussian distribution as expected for a relaxed, virialized cluster of galaxies. The

smaller foreground peak at  $z = 0.381$  ( $0.374 < z < 0.387$ , component B), by contrast, seems too wide for the small number of 46 redshifts contained in it. This impression is confirmed by Fig. 2, which plots the redshift for each galaxy versus its projected distance from the centre of Cl0024+1654<sup>1</sup>. The distribution of the galaxies in the main peak is symmetrical with respect to the central redshift line, whereas the distribution of the foreground galaxies is roughly constant at a rest frame velocity of  $\sim -3000 \text{ km s}^{-1}$  at radii larger than  $3'$  ( $600 h^{-1} \text{ kpc}$ ), but turns off towards smaller relative velocities to merge with the main distribution at smaller projected distances.

The 17 galaxies in the peak at  $z = 0.407$  are more widely dispersed across the survey field and although we cannot rule out a connection with Cl0024+1654, it seems more likely, in the light of the scenario developed in Sect. 3, that they are part of the surrounding field galaxy population.

It is remarkable that we can trace the main cluster as well as the foreground structure out to the edge of the survey field (there is only one object in the catalogue at  $r > 15'$ , a background galaxy). The virial radius for Cl0024+1654 should be around  $1 h^{-1} \text{ Mpc}$  (Girardi & Mezzetti 2001), which means that we detect a coherent structure out to three times the virial radius.

From Fig. 2 it is obvious that the central region of Cl0024+1654 is highly perturbed and it is impossible to separate components A and B within  $\sim 200''$  from the projected cluster centre. However, the redshift distribution for the central galaxies is strongly skewed towards negative velocities: except for two galaxies that are fairly isolated in redshift space, the redshift distribution at positive velocities is effectively cut off at  $\sim 1500 \text{ km s}^{-1}$ , whereas the distribution at negative velocities extends to beyond  $\sim -2500 \text{ km s}^{-1}$ , branching off into component B at  $\sim 500 h^{-1} \text{ kpc}$  from the projected cluster centre. The skew in the central redshift distribution is already apparent in the histogram given by Dressler et al. (1999) (see also Section 4).

The mean redshift of galaxies belonging to component A at projected distances  $200'' < R < 500''$  is

$$\bar{z}_A = 0.3946 \pm 0.0007 \quad . \quad (1)$$

In Fig. 3 we show the two velocity dispersion profiles for galaxies in component A with either positive or negative velocities with respect to the mean redshift  $\bar{z}_A$ , calculated in a sliding bin containing 30 galaxies. Outside  $3'$  ( $600 h^{-1} \text{ kpc}$ ) both profiles are flat at the same level of  $\sigma \approx 600 \text{ km s}^{-1}$ . The exact value from 71 galaxies at  $200'' < R < 500''$  and  $|v| < 1500 \text{ km s}^{-1}$  (both positive and negative velocities) is

$$\sigma_A = 561_{-83}^{+95} \text{ km s}^{-1} \quad . \quad (2)$$

<sup>1</sup> The coordinates in the catalogue are given relative to  $\alpha_{2000} = 00^{\text{h}}26^{\text{m}}35^{\text{s}}.70$ ,  $\delta_{2000} = 17^{\circ}09'43''.06$ . Originally, this was the position of galaxy 373, but a more accurate astrometric analysis shifted the reference point by  $0''.79$  to the south-east of this galaxy.

Both  $\bar{z}_A$  and  $\sigma_A$  were computed using the biweight estimator (Beers et al. 1990), the errors (95% confidence level) were estimated by bootstrap resampling.

The profile for galaxies with negative velocities (i. e. those moving towards us, Fig. 3) rises all the way to about  $45''$  ( $140 h^{-1} \text{ kpc}$ ), reaching a velocity dispersion of nearly  $900 \text{ km s}^{-1}$  in the innermost bin. The dispersion profile of the galaxies with positive velocities, by contrast, drops back to a value of about  $600 \text{ km s}^{-1}$  after having reached a maximum value of about  $800 \text{ km s}^{-1}$  at  $2'$  from the centre. Although the galaxy velocities used in Fig. 3 have been restricted to  $|v| < 1500 \text{ km s}^{-1}$ , the different behaviour of the profiles for galaxies with positive and negative velocities respectively reflects the skew in the central redshift distribution and indicates the possible presence of a bulk motion component towards us in the central galaxy distribution.

The velocity dispersion for component B in the same radial distance range as used in Eq. 2 is  $\sigma_B = 554_{-304}^{+175} \text{ km s}^{-1}$  based on 15 redshifts. Given that the number of galaxies in component A is almost five times as large as the number in component B it is hardly conceivable that both components should have the same velocity dispersion – their mass-to-light ratios would be extremely different. Component B is certainly not a virialized group or cluster.

Fig. 2 shows the theoretical escape velocities for masses of  $1, 3$  and  $5 \times 10^{14} M_{\odot}$  enclosed in a sphere of radius  $R$ . Although these lines are merely indicative due to the assumption of spherical symmetry and the unknown tangential velocity components, it is safe to say that the galaxies in component B outside, say,  $600 h^{-1} \text{ kpc}$  are not bound to the main cluster component, unlike the negative tail of the skewed central galaxy distribution.

### 2.3. Equivalent width distribution

Fig. 4 shows scatterplots of the most important observables from the spectroscopic catalogue for the 282 galaxies with redshift  $0.37 < z < 0.402$ . The bimodal redshift distribution is apparent in the distributions of  $V-I$  colour, the equivalent widths of O II and H  $\delta$  and the strength of the  $4000 \text{ \AA}$  break (panels 10, 4, 5, and 6 respectively), as well as in the radial distance distribution (panel 13, which is a reprise of Fig. 2). In the colour distribution (panel 10), the two modes merge at  $V-I \simeq 2$ , typical of the red early-type galaxy population; the red galaxies are crowded at small distances from the cluster centre (panel 14). A similar trend is visible in the distribution of the  $4000 \text{ \AA}$  with radial distance (panel 3). On the other hand, no such crowding is found when plotting  $EW([\text{O II}])$  versus  $V-I$  (panel 7), as is to be expected since central cluster populations have few star-forming regions and are dominated by older red stars. As expected, the bluest galaxies in the cluster show the strongest [O II] emission. [O II] equivalent widths are distributed fairly homogeneously with clustercentric distance (panel 1), although a more precise analysis must

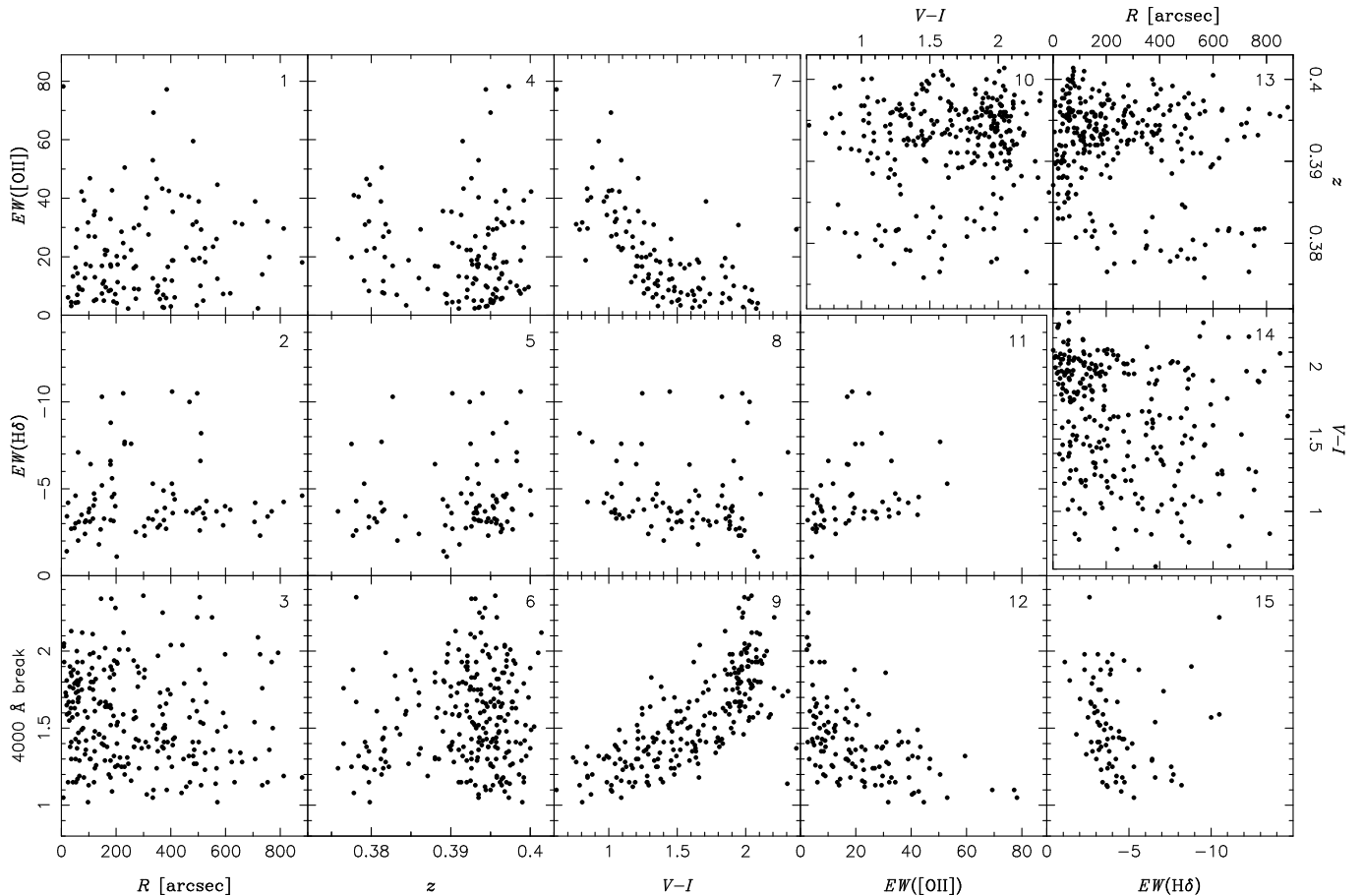


**Fig. 4.** Matrix of scatter plots showing the most important observables (projected radial distance  $R$ , redshift  $z$ , colour  $V - I$ , equivalent widths for  $[\text{O II}]$  and  $\text{H}\delta$  as well as the strength of the  $4000 \text{ \AA}$  break) for the galaxies in the vicinity of the cluster redshift.

take into account the fact that the survey samples the field in an inhomogeneous way, completeness being largest in the cluster centre and generally decreasing with projected distance (see Paper I, Fig. 7).

In Tables 1 and 2 we classify the galaxies into spectral types using our measured values for the equivalent widths of  $[\text{O II}]$ ,  $\text{H}\delta$  and the  $4000 \text{ \AA}$  break (see Paper I for details on how these values are defined and measured). The numbers are the percentages  $p$  of galaxies belonging to each class in each sample. The errors are the standard deviations  $\sqrt{Np(1-p)}$  of the normal distribution asymptotic to the binomial distribution with sample size  $N$  and probability  $p$  for large  $N$ . The classification follows Balogh et al. (1999): K+A galaxies show strong  $\text{H}\delta$  absorption, but no  $[\text{O II}]$  emission, whereas A+em galaxies show both  $\text{H}\delta$  absorption and  $[\text{O II}]$  emission; the limiting values are specified in Table 1. The star-forming galaxies of type SF/SSB (“star-forming” and “short star-burst”, here treated as one class) show strong  $[\text{O II}]$  emission, but no  $\text{H}\delta$  absorption. Passive galaxies, finally, show neither  $[\text{O II}]$  emission nor  $\text{H}\delta$  absorption.

In the classification by  $\text{H}\delta$  and the  $4000 \text{ \AA}$  break (Table 2) “bHDS” and “rHDS” refer to blue and red  $\text{H}\delta$  strong galaxies, depending on whether the break is weaker or

stronger than  $1.5$  (Balogh et al. 1999). Galaxies with no  $\text{H}\delta$  are again classified as SF/SSB (weak break) or passive (strong break). Again the limiting values follow Balogh et al. (1999) and are specified in Table 2.

We consider four samples of galaxies according to redshift and projected spatial position; the sample boundaries are marked by the dotted lines in Fig. 2. “Field” includes all the galaxies in the sample with redshifts  $0 < z < 0.55$  without the cluster galaxies,  $0.372 < z < 0.402$  (the upper limit here is the same as for the field sample in Balogh et al. (1999)). “Centre” includes galaxies within a radial distance of  $1 h^{-1} \text{ Mpc}$  (corresponding roughly to the virial radius) from the projected cluster centre, with relative velocities  $1.5 R [h^{-1} \text{ kpc}] - 3000 < v [\text{km s}^{-1}] < 1500$ . The lower limiting line is a visually motivated demarcation from component “B”, which comprises the galaxies with  $z > 0.372$  and  $v < -1500 \text{ km s}^{-1}$  ( $z < 0.388$ ) and below this line. Adding the galaxies between this line and  $v = -1500 \text{ km s}^{-1}$  to component B does not significantly change the numbers in Tables 1 and 2. Component “A” in the tables includes all galaxies outside  $1 h^{-1} \text{ Mpc}$  and  $|v| < 1500 \text{ km s}^{-1}$ .

Looking first at the classification by  $[\text{O II}]$  and  $\text{H}\delta$  (Table 1), we find that our fractions for the centre and

**Table 1.** Distribution of spectral types: classification by [O II] vs. H $\delta$ . The fraction of galaxies of a given spectral type is listed as the percentage of the total number of galaxies in the subsample (the total number is given in parentheses). See text and Fig. 2 for the definitions of the samples.

Spectral Type	Definition	This work				Balogh et al. (1999)	
		Centre (183)	A (64)	B (35)	Field (275)	Cluster	Field
K+A	H $\delta < -5 \text{ \AA}$ , [O II] $< 5 \text{ \AA}$	2 $\pm$ 1	3 $\pm$ 2	0.0	4 $\pm$ 1	4	2
A+em	H $\delta < -5 \text{ \AA}$ , [O II] $> 5 \text{ \AA}$	3 $\pm$ 1	6 $\pm$ 3	11 $\pm$ 5	3 $\pm$ 1	4	10
SF/SSB	H $\delta > -5 \text{ \AA}$ , [O II] $> 5 \text{ \AA}$	23 $\pm$ 3	42 $\pm$ 6	57 $\pm$ 8	53 $\pm$ 3	24	47
passive	H $\delta > -5 \text{ \AA}$ , [O II] $< 5 \text{ \AA}$	72 $\pm$ 3	48 $\pm$ 6	31 $\pm$ 7	40 $\pm$ 3	67	41

**Table 2.** Distribution of spectral types: classification by H $\delta$  and the 4000 $\text{\AA}$  break. The structure of the tale is the same as for Table 1.

Spectral Type	Definition	This work				Balogh et al. (1999)	
		Centre (148)	A (60)	B (33)	Field (225)	Cluster	Field
bHDS	H $\delta < -5 \text{ \AA}$ , br $< 1.5$	3 $\pm$ 1	3 $\pm$ 2	9 $\pm$ 5	7 $\pm$ 1	5	7
rHDS	H $\delta < -3 \text{ \AA}$ , br $> 1.5$	8 $\pm$ 2	17 $\pm$ 5	9 $\pm$ 5	5 $\pm$ 1	10	11
SF/SSB	H $\delta > -5 \text{ \AA}$ , br $< 1.5$	34 $\pm$ 3	50 $\pm$ 6	67 $\pm$ 8	56 $\pm$ 3	12	33
passive	H $\delta > -3 \text{ \AA}$ , br $> 1.5$	55 $\pm$ 4	30 $\pm$ 6	15 $\pm$ 6	32 $\pm$ 3	74	45

field are in good agreement with the numbers for cluster and field found by Balogh et al. (1999), demonstrating the comparability of our equivalent width measurements. The distribution of spectral types in the foreground component B is very close to the distribution in the field with even a hint of an excess of star-forming galaxies. The distribution in the periphery of component A is between those for B/field and the distribution in the centre.

Our numbers in the classification by H $\delta$  and the 4000  $\text{\AA}$  break are not directly comparable to those in Balogh et al. (1999) because our definition of the wavelength regions defining the continuum on both sides of the break differs from theirs. Also, for galaxies at  $z = 0.3942$ , i. e. at the cluster redshift, the 4000  $\text{\AA}$  break coincides with the [O I] sky emission line at  $\lambda = 5577 \text{ \AA}$ , which impairs the measurement of the strength of the break in some cases. However, the general trend of a larger fraction of red galaxies in the cluster as compared to field is also present in our data. As before the distribution in component B is close to that in the field with the excess of star-forming galaxies being even somewhat more pronounced. Again the distribution in component A is between those of the field and the cluster centre.

#### 2.4. Spatial galaxy distribution

Knowing redshifts for a large number of cluster members allows us to draw accurate maps of the projected galaxy number density. This is done in Fig. 5, where we show maps for the cluster components A and B, as well as for field galaxies with  $0.1 < z < 0.35$ .

The maps were drawn using the generalized nearest neighbour method (Silverman 1986): At each point the mean quadratic radius  $R_m^2 = (R_N^2 + R_{N+1}^2) / 2$  was deter-

mined, where  $R_N$  and  $R_{N+1}$  are the distances to the  $N^{\text{th}}$  and  $(N+1)^{\text{th}}$  nearest galaxies in the redshift range, respectively. The density is then given by

$$n = \frac{1}{C_s} \frac{N}{\pi R_m^2}, \quad (3)$$

where  $C_s$  is the spatial completeness of the spectroscopic catalogue, as determined in Paper I (Fig. 7). For the main cluster component A we used  $N = 10$ , for the foreground component B and the field we chose  $N = 5$  due the smaller number of galaxies. In the map of component A,  $R_m \simeq 30''$  in the cluster centre,  $\simeq 50''$  at the 50% contour and increases to  $\simeq 150''$  at the 10% contour. In the map of component B, which has the same contour levels as the map of A but different  $N$ , the corresponding values are  $R_m \simeq 50''$  in the centre of the field, rising to  $\simeq 500''$  in the most sparsely sampled external regions. In the field map, the smoothing radius  $R_m$  varies between  $\simeq 100''$  and  $\simeq 250''$ .

The map of the field galaxies (right panel in Fig. 5) is fairly flat, indicating that the completeness correction  $C_s$  is satisfactory. Peaks in these maps thus correspond to true galaxy density maxima and are not biased by the inhomogeneous sampling of the survey area. The left and the centre panels show components A and B respectively, with the limit between those two chosen as  $z = 0.387$ . Due to this limit (dictated by the gap between the two components at large projected distances) part of the skewed central galaxy distribution is included in component B and thus accounts for the central peak in the map of this component. More importantly however, the galaxies in the outer regions of component B are spread isotropically around the cluster centre, indicating that we are looking along an axis of symmetry of the system.

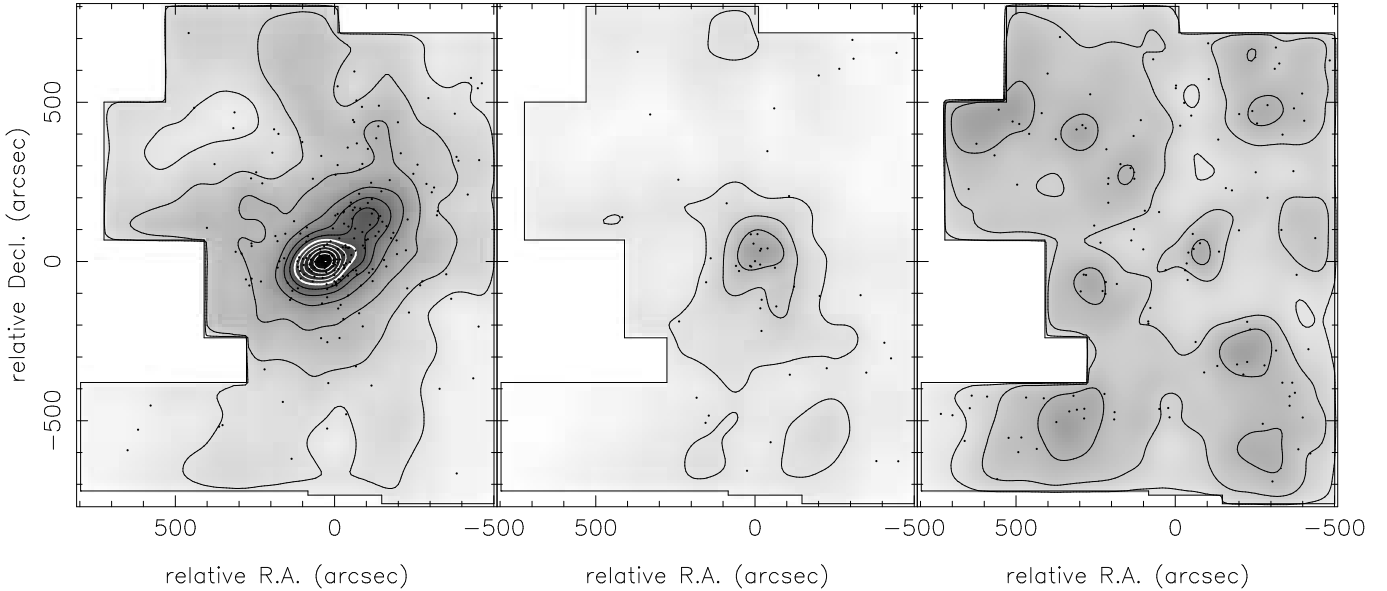


**Fig. 5.** Galaxy number density maps for (a) component A ( $0.388 < z < 0.402$ , 237 galaxies), (b) component B ( $0.37 < z < 0.388$ , 46 galaxies) and (c) the “field” ( $0.1 < z < 0.35$ , 141 galaxies), estimated with the generalized nearest neighbour method with 10 neighbours for map (a) and 5 neighbours for maps (b) and (c). The maps are divided by the completeness map (see Paper I) and smoothed with a Gaussian with  $\sigma = 30''$ . The grey scales are the same for all three maps. The lowest density contour lines are at 2% and 5%, normalized to the maximum density in the cluster component A (left panel). The remaining contours are spaced in steps of 10%. For densities below 50% the contours are drawn in black, for higher densities in white. The 50% contour is marked by a bold white line.

The map of the main component A shows a clear extension of the galaxy distribution towards the northwest to a distance of  $100'' - 150''$ . This extension is visible in images of Cl0024+1654 and we show here that the galaxies contained in it lie at the redshift of the main cluster. The ROSAT HRI image of Cl0024+1654 shows an X-ray source (S1 in Soucail et al. 2000) at a distance of  $70''$  from the cluster centre in the same direction as the extension. S1 is a compact source although it is not clear whether it actually is a point source or whether it is just resolved. There are several possible optical counterparts in the optical image, one a cluster galaxy at  $z = 0.4017$  and another one a foreground galaxy at  $z = 0.2132$ . Under the assumption that S1 is at the cluster redshift, we find a luminosity of  $L_X = 8 \times 10^{12} h^{-2} \text{ erg s}^{-1}$  in the ROSAT band  $[0.1 - 2.4] \text{ keV}$ , assuming a thermal spectrum with a temperature of  $2 \text{ keV}$ . This luminosity is typical for small clusters or groups of galaxies. Further observations taking advantage of the increased spatial and spectral resolution of the CHANDRA and XMM satellites are however necessary to interpret this source.

### 3. A high speed collision?

In general, a redshift difference between well-separated clusters at cosmological distances is a combination of a cosmological redshift difference due to the proper distance between the clusters along the line of sight and a Doppler shift due to the relative velocities of the two clusters. These two effects cannot be disentangled quantitatively;

however, on the basis of plausibility arguments we can show that the Doppler shift is likely the relevant effect in the case of Cl0024+1654.

If we first assume that the redshift difference is due to the spatial separation of components A and B, then  $\Delta z = 0.014$  translates to a proper distance along the line of sight of  $\sim 20 h^{-1} \text{ Mpc}$  at the epoch corresponding to  $z = 0.395$  in an Einstein-de Sitter universe. Since the redshift difference decreases towards the projected centre of Cl0024+1654, we would have to assume that the centre of cluster B moves with a relative peculiar velocity of  $\sim 1500 \text{ km s}^{-1}$  with respect to its periphery towards cluster A, presumably due to the latter’s gravitational pull. However, the transverse size of the infalling core of cluster B is only  $\sim 500 h^{-1} \text{ kpc}$ , much smaller than the distance from cluster A. If cluster B were indeed sitting at a distance of  $\sim 20 h^{-1} \text{ Mpc}$  in front of cluster A, we would expect it to fall towards cluster A as a whole with no differential effects on central and external galaxies.

A possible solution to the observed redshift distribution is that a group or cluster has undergone a near radial collision with Cl0024+1654 and we are now viewing the merging system along the direction of the impact. In fact, several characteristic parameters of the collision are fairly well constrained by the observed redshift distribution. The relative velocity of the two subclusters is given by the redshift difference of components A and B and is thus of order  $3000 \text{ km s}^{-1}$ . Those parts of the smaller cluster B that pass through the centre of A are more strongly decelerated in the direction of the collision than its outer parts due

**Fig. 6.** The initial and final particle configurations used to simulate the two colliding clusters. The grey scale indicates the local density of dark matter within the box of length 12 Mpc.

to stronger dynamical friction and they therefore show a smaller redshift difference. A tidal gravitational shock during the crossing scatters the outer galaxies of both clusters to large projected distance, thus increasing the extent of the cluster halos beyond their nominal virial radius. If the transverse velocity imparted on a galaxy that is now found at a radial distance of  $3h^{-1}$  Mpc is  $1000 \text{ km s}^{-1}$ , then the time since core crossing is about 3 Gyrs, and the separation between the cores of the two clusters is roughly 5 Mpc.

The main unknown in this scenario is the mass ratio between the subclusters. There are two possible scenarios for this collision:

(i) A small group has passed through the core of Cl0024+1654 and has been completely disrupted and scattered by the cluster’s tidal force. In this case the main body of Cl0024+1654 is unperturbed and we do not observe a concentration of foreground galaxies belonging to the original group because the system has been completely unbound and is scattered to large distances perpendicular to the main cluster.

(ii) A massive cluster of approximately 50% of the mass of Cl0024+1654 collided and passed through the core of Cl0024+1654 roughly 3 Gyr ago. This collision is insufficient to completely disrupt the impacting cluster but its outer galaxies are scattered to large projected distances. The remaining bound core of the colliding cluster undergoes sufficient dynamical friction to turn its orbit around and in redshift space it appears to lie at a similar distance to Cl0024+1654.

Both of these scenarios can reproduce the main features of the observed redshift distribution. However, the massive collision scenario is more interesting because of the possibility of resolving both the mass discrepancy problem and the conflict between the central density structure of Cl0024+1654 and predictions of hierarchical clustering models.

The mass reconstructions of Cl0024+1654 (Tyson et al. 1998; Broadhurst et al. 2000) using the positions of multiple images of a gravitationally lensed background galaxy show a projected mass of  $1.3 \times 10^{14} h^{-1} M_{\odot}$  within  $106 h^{-1} \text{ kpc}$  and a central surface mass density of  $7900 h M_{\odot} \text{ pc}^{-2}$ . For a singular isothermal halo extending to  $r_{200}/\text{kpc} \approx \sqrt{2} \sigma_{1d}/(\text{km s}^{-1})$  this implies a characteristic velocity dispersion larger than  $1500 \text{ km s}^{-1}$  in order to explain the projected mass. This is inconsistent with the observations presented in this paper.

Dark matter halos in cold dark matter (CDM) type models are shallower than isothermal in their centres. In order to reproduce the observed projected mass from a single cluster we are forced to adopt a cluster halo with a very large characteristic velocity. As Shapiro & Iliev (2000) point out, it is very difficult to obtain a consistent mass model for this cluster, especially in the context

of hierarchical clustering models. In order to reproduce the observed projected mass a CDM halo with velocity dispersion of  $2200 \text{ km s}^{-1}$  is required, well over twice as high as the observed value. A second problem for hierarchical models is that Tyson et al. (1998) infer a very shallow central density profile for this cluster, much flatter than the cuspy density profiles found for clusters in CDM type models (Ghigna et al. 2000). The central core of Cl0024+1654 has frequently been used to constrain the nature of dark matter and to argue for alternative candidates to CDM (Spergel & Steinhardt 2000; Hogan & Dalcanton 2000; Moore et al. 2000).

A high speed encounter between two similar mass clusters can explain all of these observations and reconcile the above mass discrepancies. We now explore this scenario using high resolution numerical simulations of colliding dark matter halos to study the evolution of the mass distribution. We construct two equilibrium CDM halos with virial masses  $9.5 \times 10^{14} M_{\odot}$  and  $5.0 \times 10^{14} M_{\odot}$  with peak circular velocities  $v_{\text{peak}} = 1600$  and  $1300 \text{ km s}^{-1}$  and concentrations  $c = 5$  and  $c = 7$  respectively. Their initial separation is 3 Mpc and relative velocity is  $-3000 \text{ km s}^{-1}$ . The particle mass is set to  $5 \times 10^9 M_{\odot}$  and we use an equivalent Plummer force softening of 5 kpc.

After the collision we find that the outer regions of the smaller cluster have become unbound and are streaming radially away from the impact location. The impulse velocity perpendicular to the encounter is of the order  $1000 \text{ km s}^{-1}$ . Snapshots of the initial and final times are shown in Fig. 6. The peak circular velocities of the bound components have fallen to  $1430$  and  $1140 \text{ km s}^{-1}$  whilst the central 1D velocity dispersions have reduced to  $930$  and  $710 \text{ km s}^{-1}$  from initial values of  $1033$  and  $883 \text{ km s}^{-1}$  respectively. At the final time we find a total mass within a cylinder of radius  $106 \text{ kpc}$  of  $8.0 \times 10^{13} M_{\odot}$ .

The redshift distribution of 10 000 randomly selected particles at the final time is shown in the right hand panel in Fig. 7. This is not a perfect match to the observational data but the main features are present: we see a foreground component of “galaxies” that span large projected distances from the central region of Cl0024+1654. This component is separated by  $\approx 3000 \text{ km s}^{-1}$  in redshift space from the main component. The smaller cluster bound core is moving away from the main cluster at  $\approx 1000 \text{ km s}^{-1}$  – the reduction in speed from the initial velocity is due to dynamical friction. A better agreement would result if the impacting cluster was slightly more massive in which case it would suffer more friction and would be seen nearly at rest compared to the main component. Also note that we are plotting “dark matter particles” not “galaxies”. Of course the initial configuration shown in the left panel in Fig. 7 also displays a bimodal distribution of redshifts. However, this configuration is more symmetric than either the final simulated configuration or the observed redshift

distribution; also, the radial extent, in particular of the foreground (in redshift space) component, is much smaller than observed.

The energy from the impulsive tidal shock has been transferred into kinetic energy of the particles, heating and expanding the cold central cores of the clusters. This leads to a flattening of the physical and projected density profiles. In Fig. 8 we show the projected surface mass density profile before and after the encounter. The initial profiles are cuspy, CDM type density profiles whereas the final profiles have nearly constant density cores in good agreement with that inferred from the mass reconstruction (Tyson et al. 1998, their Figure 4). The central surface mass density is  $4000 M_{\odot} \text{pc}^{-2}$  which is very close to the value obtained by Tyson et al. for  $H_0 = 50 \text{ km s}^{-1} \text{Mpc}^{-1}$ . The total projected mass within the central 106 kpc is about 30% lower than obtained by Broadhurst et al. (2000) which could be reconciled by using a more massive encounter and/or properly including the baryonic matter.

#### 4. Discussion

The fact that Cl0024+1654 is not a simple relaxed cluster invalidates attempts to determine its mass with methods which rely on the assumption of dynamical equilibrium.

The large velocity dispersion of  $\sigma \approx 1200 \text{ km s}^{-1}$  found by Dressler & Gunn (1992) and Dressler et al. (1999) (hereafter D99) was based on galaxies within  $5'$  from the projected cluster centre. As shown in Fig. 9, there is no direct evidence for the bimodality of Cl0024+1654 when attention is restricted to the central regions of the cluster. This is still true with the larger number of galaxy spectra used here: Whereas our catalogue contains about 85% more redshifts in this area than D99, the general shape of the histogram is the same. Both histograms are strongly skewed towards low redshifts, thus indicating the presence of substructure (Ashman et al. 1994). The bimodality of the redshift distribution however becomes apparent only when galaxies at larger projected distances from the cluster centre are included.

As argued in Section 2.2, part of the formal velocity dispersion of the central galaxy distribution is due to bulk motion and thus not indicative of the cluster's mass. At projected distances  $> 3'$  the components A and B separate and the velocity distribution of component A is regular with a dispersion of  $\sim 600 \text{ km s}^{-1}$ . If this were the velocity dispersion of a relaxed cluster, it would have only about a quarter of the mass previously estimated for Cl0024+1654 (Schneider et al. 1986). However, in the light of the merger scenario presented in Section 3 we caution against any mass estimates from galaxy kinematics for this cluster and generally for clusters showing significantly skewed redshift distributions in their core.

The X-ray data are difficult to interpret in the context of two clusters projected along the line-of-sight several Gyr after a head-on collision. During the collision, hydrostatic equilibrium in the gas component of the cluster(s) breaks down and the X-ray luminosity and emission-

weighted temperature fluctuate considerably (by up to a factor of 10 for  $L_X$ ) and rapidly as a consequence of the formation of shock waves and repeated expansion and compression of the core gas (Takizawa 1999; Ricker & Sarazin 2001; Ritchie & Thomas 2001). After several Gyr however, shocks have dissipated and the gas settles down to an equilibrium configuration. The cited hydrodynamic simulations of cluster mergers consider collision speeds of about  $1000 \text{ km s}^{-1}$ ; in this case the dark matter cores separate to distances of only a couple of Mpc before turning around and eventually merging into one clump. In a high-speed collision, however, the collisionless dark matter cores of the two clusters separate to large distance before turning around. The gas, due to its collisional nature should experience stronger interaction during the first crossing and thus behave quite differently from the dark matter/galaxies and possibly also from what low-speed collision simulations predict. Ricker & Sarazin (2001) observe a slight segregation between the gas and the dark matter cores in their simulations. This effect should be more pronounced in a high-speed collision. Given the measured values for Cl0024+1654,  $T_X = 5.7^{+4.9}_{-2.1} \text{ keV}$  and  $L_X = 6.8 \times 10^{43} h^{-2} \text{ erg s}^{-1}$  (Soucail et al. 2000), the gas does not actually seem too far away from the  $L_X - T_X$  relation of Markevitch (1998); it is slightly too hot for its luminosity. An increase in gas entropy due to the collision would be sufficient to explain this, however it is doubtful that the gas in Cl0024+1654 is in any equilibrium state. Detailed inclusion of a hydrodynamic treatment of the gas component in simulations of high-speed collisions is necessary to answer this question.

Gravitational lensing by clusters of galaxies does not rely on the matter in the clusters being in dynamical equilibrium. However, gravitational lensing measures the weighted integral of all the mass between the observer and the source, and the interpretation of the measured mass value thus depends on the detailed distribution of mass along the line-of-sight. In the case of Cl0024+1654, the mass derived from the lensing analyses includes contributions from both component A and B, and is therefore too large if interpreted as representing the mass of a single cluster. However, the projected mass profile for the post-merger system seen in our simulations shows two characteristics which are testable by gravitational lensing analyses of Cl0024+1654: At small scales of several 10's kpc, the profile shows a flat core which is consistent with strong lensing mass models (Tyson et al. 1998). On large scales the profile is significantly flatter than the initial CDM profile, falling only as  $r^{-2.5}$  out to  $\sim 3 \text{ Mpc}$ . Previous weak lensing analyses on Cl0024+1654 have not attempted a detailed reconstruction of the mass profile. Bonnet et al. (1994) and van Waerbeke et al. (1997) derived shear maps from ground-based data on the north-east quadrant of the cluster, Smail et al. (1997) were restricted to the small field of view of HST/WFPC2. The shear pattern found by Bonnet et al. (1994) is compatible with an isothermal sphere profile,  $\rho \propto r^{-2}$  out to  $3 h^{-1} \text{ Mpc}$ . A sparsely sampled HST/WFPC2 mosaic consisting of 38 pointings

out to a distance of  $2.5 h^{-1}$  Mpc from the cluster centre has recently been obtained and a weak lensing analysis is currently under way (Treu 2001). These data will allow to probe the cluster's projected radial mass profile accurately to the edge of the survey field.

Head-on mergers are not easy to identify as such, yet most cluster selection techniques are prone to preferentially select such cases. The influence of projection effects on optical searches for galaxy overdensities has long been recognized; this is particularly important for merging clusters or clusters that are about to collide in the near future. These clusters are at almost the same distance and cannot be separated by photometric redshift techniques. Flux-limited X-ray samples of clusters of galaxies might be biased towards merging systems due to the strong if short-lived increase in X-ray luminosity just after core crossing (Ritchie & Thomas 2001). Even weak-lensing surveys for clusters of galaxies are subject to this bias due to the increased projected mass density in merging clusters of galaxies.

On-going cluster mergers are fairly easily detectable if the line-of-sight is perpendicular to the merger axis. In 30% of the observed cluster mergers, however, the merger axis should be aligned with the line-of-sight to less than  $45^\circ$ . A quantitative analysis of the magnitude of the bias towards merging systems should come from cosmological numerical simulations. A high-speed collision several Gyrs after the first core crossing, such as proposed here for Cl0024+1654, on the other hand is difficult to recognize as such if viewed sideways, although it might possibly be distinguished from an ordinary double cluster by the presence of gas between the cluster cores, or by a departure of their mass profiles from "standard" profiles.

## 5. Conclusions

In the present paper we have analyzed the galaxy distribution in the cluster of galaxies Cl0024+1654, based on  $\sim 300$  galaxy redshifts and projected positions. The cluster, which was previously regarded as a prototype of a massive relaxed cluster at intermediate redshift, turns out to have a fairly complicated structure, showing a strongly skewed redshift distribution in its central parts and two well-separated components at larger projected distances out to  $\sim 3 h^{-1}$  Mpc. We interpret this peculiar redshift-space distribution as the result of a high-speed head-on collision of two clusters of galaxies, the merger axis being very nearly parallel to the line-of-sight. Using a numerical simulation we have shown that it is possible to explain the observed redshift distribution with a high-speed collision of two rather massive clusters of galaxies with a mass ratio of about 2:1. Apart from reproducing the spatial/redshift distribution of the cluster galaxies, this scenario also produces a projected mass distribution which is very close to that derived by Tyson et al. (1998) from the quintuple arc system observed in Cl0024+1654. Since it is thus possible to produce a mass distribution with a flat core from the merger of two CDM halos this eliminates one of the main

arguments against simple non-interacting cold dark matter as the dynamically dominant component in clusters of galaxies (Spergel & Steinhardt 2000). It is possible to model the strong lens configuration of Cl0024+1654 using a CDM like mass profile with a central cusp (Broadhurst et al. 2000), however this predicts a velocity dispersion which is too high, even compared to the observed central velocity dispersion of  $\sim 1200 \text{ km s}^{-1}$  (Shapiro & Iliev 2000).

The relative velocity of the clusters of  $\sim 3000 \text{ km s}^{-1}$  implied by the redshift distribution in Cl0024+1654 is very high. Observations and simulations find mean peculiar velocities for clusters of order  $500 \text{ km s}^{-1}$  (Bahcall & Oh 1996; Giovanelli et al. 1998; Gibbons et al. 2001; Colberg et al. 2000). Still, colliding clusters can reach relative velocities of about  $3000 \text{ km s}^{-1}$  at separations of about 1 Mpc (Sarazin 2001). Markevitch et al. (2001) have recently found a bow shock in the galaxy cluster 1E0657-56 which implies a relative speed of 3000 to  $4000 \text{ km s}^{-1}$  for the collision. Cl0024+1654 is still an extraordinary but not an impossible system.

We stress again that the merger scenario presented here is not unique and for example a collision involving clusters with a larger mass ratio might also be able to reproduce the observed redshift/space distribution. The main difference to the 2:1 mass ratio scenario is that the core of the smaller cluster or group would not survive such a collision, rather the whole cluster would be destroyed and scattered apart. Whereas cluster mergers with different mass ratios show distinct observational characteristics when viewed sideways, the distinction between these two cases is difficult when viewed head-on.

The distribution of spectral types in the foreground component B is more akin to the general field population than to a cluster population. In the context of our merger scenario, these would correspond to the outer regions of the smaller cluster which have become unbound during the impact. Even initially, these galaxies would probably not correspond to a fully transformed cluster galaxy population. In addition, the impact might have triggered some additional star formation in these galaxies. Remembering that Cl0024+1654 was one of the most distant clusters in which the Butcher-Oemler effect was detected (Butcher & Oemler 1984; Dressler et al. 1985), this may add a new view on this effect: The fact that  $\sim 40\%$  of the bright galaxies in the cluster are emission line galaxies ( $[\text{O II}] > 5 \text{ \AA}$ ) has a natural interpretation in the collision scenario. The spectral distribution of the galaxies in component A (and centre) are also perturbed by the collision with a possible excess of rHDS and SF/SBB; rHDS galaxies may represent the result of a starburst induced during the early stages of the interaction.

Whatever the exact explanation of the complicated redshift/space structure of Cl0024+1654, the fact remains that the cluster is disturbed and not in an equilibrium state, invalidating most attempts at estimating its mass. This fact is not easily discernible in the galaxy distribution or the X-ray surface brightness distribution and con-

sequently similar cases might easily go unnoticed in the context of large samples of high-redshift clusters of galaxies, introducing scatter e. g. in the mass-temperature relation. Redshift surveys seem to be the most secure way of detecting head-on mergers, in particular if they cover a wide field, although a skew in the central redshift dispersion should be taken as a warning sign for significant line-of-sight structure.

*Acknowledgements.* OC thanks the European Commission for generous support under grant number ER-BFM-BI-CT97-2471 and the Institute for Astronomy in Honolulu, in particular Harald Ebeling, for kind hospitality. JPK thanks CNRS for support. We also acknowledge support from the UK-French ALLIANCE collaboration programme 0161XM.

## References

- Ashman, K. A., Bird, C. M., & Zepf, S. E. 1994, *AJ*, 108, 2348
- Bahcall, N. A. & Oh, S. P. 1996, *ApJ*, 462, L49
- Balogh, M. L., Morris, S. L., Yee, H. K. C., Carlberg, R. G., & Ellingson, E. 1999, *ApJ*, 527, 54
- Beers, T. C., Flynn, K., & Gebhardt, K. 1990, *AJ*, 100, 32
- Bonnet, H., Mellier, Y., & Fort, B. 1994, *ApJ*, 427, L83
- Broadhurst, T., Huang, X., Frye, B., & Ellis, R. S. 2000, *ApJ*, 534, L15
- Butcher, H. & Oemler, Jr., A. 1984, *ApJ*, 285, 426
- Colberg, J. M., White, S. D. M., MacFarland, T. J., Jenkins, A., Pearce, F. R., Frenk, C. S., Thomas, P. A., & Couchman, H. M. P. 2000, *MNRAS*, 313, 229
- Czoske, O., Kneib, J.-P., Soucail, G., Bridges, T. J., Mellier, Y., & Cuillandre, J.-C. 2001, *A&A*, 372, 391
- Dressler, A. & Gunn, J. E. 1992, *ApJS*, 78, 1
- Dressler, A., Gunn, J. E., & Schneider, D. P. 1985, *ApJ*, 294, 70
- Dressler, A., Smail, I., Poggianti, B. M., Butcher, H., Couch, W. J., Ellis, R. S., & Oemler, Jr., A. 1999, *ApJS*, 122, 51
- Ghigna, S., Moore, B., Governato, F., Lake, G., Quinn, T., & Stadel, J. 2000, *ApJ*, 544, 616
- Gibbons, R. A., Fruchter, A. S., & Bothun, G. D. 2001, *AJ*, 121, 649
- Giovanelli, R., Haynes, M. P., Salzer, J. J., Wegner, G., da Costa, L. N., & Freudling, W. 1998, *AJ*, 116, 2632
- Girardi, M. & Mezzetti, M. 2001, *ApJ*, 548, 79
- Hogan, C. J. & Dalcanton, J. J. 2000, *Phys. Rev. D*, 62, 063511
- Kassiola, A., Kovner, I., & Fort, B. 1992, *ApJ*, 400, 41
- Markevitch, M. 1998, *ApJ*, 504, 27
- Markevitch, M., Gonzalez, A. H., David, L., Vikhlinin, A., Murray, S., Forman, W., Jones, C., & Tucker, W. 2001, *astro-ph/0110468*
- Markevitch, M., Ponman, T., Nulsen, P. E. J., Bautz, M. W., Burke, D. J., David, L. P., Davis, D., Donnelly, R. H., Forman, W. R., Jones, C., Kaastra, J., Kellogg, E., Kim, D.-W., Kolodziejczak, J., Mazzotta, P., Pagliaro, A., Patel, S., Van Speybroeck, L., Vikhlinin, A., Vrtník, J., Wise, M., & Zhao, P. 2000, *ApJ*, 541, 542
- Markevitch, M. & Vikhlinin, A. 2001, *astro-ph/0105093*
- Mazzotta, P., Markevitch, M., Vikhlinin, A., Forman, W. R., David, L. P., & VanSpeybroeck, L. 2001, *ApJ*, 555, 205
- Miralda-Escudé, J. & Babul, A. 1995, *ApJ*, 449, 18
- Moore, B., Gelato, S., Jenkins, A., Pearce, F. R., & Quilis, V. 2000, *ApJ*, 535, L21
- Moore, B., Governato, F., Quinn, T., Stadel, J., & Lake, G. 1998, *ApJ*, 499, L5
- Navarro, J. F., Frenk, C. S., & White, S. D. M. 1997, *ApJ*, 490, 493
- Ricker, P. M. & Sarazin, C. L. 2001, *astro-ph/0107210*
- Ritchie, B. W. & Thomas, P. A. 2001, *astro-ph/0107374*
- Sarazin, C. L. 2001, in *Merging Processes in Clusters of Galaxies*, ed. L. Feretti, I. M. Gioia, & G. Giovannini (Kluwer, Dordrecht), *astro-ph/0105418*
- Schneider, D. P., Dressler, A., & Gunn, J. E. 1986, *AJ*, 92, 523
- Shapiro, P. R. & Iliev, I. T. 2000, *ApJ*, 542, L1
- Silverman, B. W. 1986, *Density Estimation for Statistics and Data Analysis*, Monographs on Statistics and Applied Probability (London: Chapman and Hall)
- Smail, I., Dressler, A., Kneib, J.-P., Ellis, R. S., Couch, W. J., Sharples, R. M., & Oemler, Jr., A. 1996, *ApJ*, 469, 508
- Smail, I., Ellis, R. S., Dressler, A., Couch, W. J., Oemler, Jr., A., Sharples, R. M., & Butcher, H. 1997, *ApJ*, 479, 70
- Soucail, G., Ota, N., Böhringer, H., Czoske, O., Hattori, M., & Mellier, Y. 2000, *A&A*, 355, 433
- Spergel, D. N. & Steinhardt, P. J. 2000, *Phys. Rev. Lett.*, 84, 3760
- Takizawa, M. 1999, *ApJ*, 520, 514
- Treu, T. 2001, *SESTO conference*
- Tyson, J. A., Kochanski, G. P., & Dell’Antonio, I. P. 1998, *ApJ*, 498, L107
- van Waerbeke, L., Mellier, Y., Schneider, P., Fort, B., & Mathez, G. 1997, *A&A*, 317, 303
- Vikhlinin, A., Markevitch, M., & Murray, S. S. 2001, *ApJ*, 551, 160
- Wu, X.-P., Chiueh, T., Fang, L.-Z., & Xue, Y.-J. 1998, *MNRAS*, 301, 861

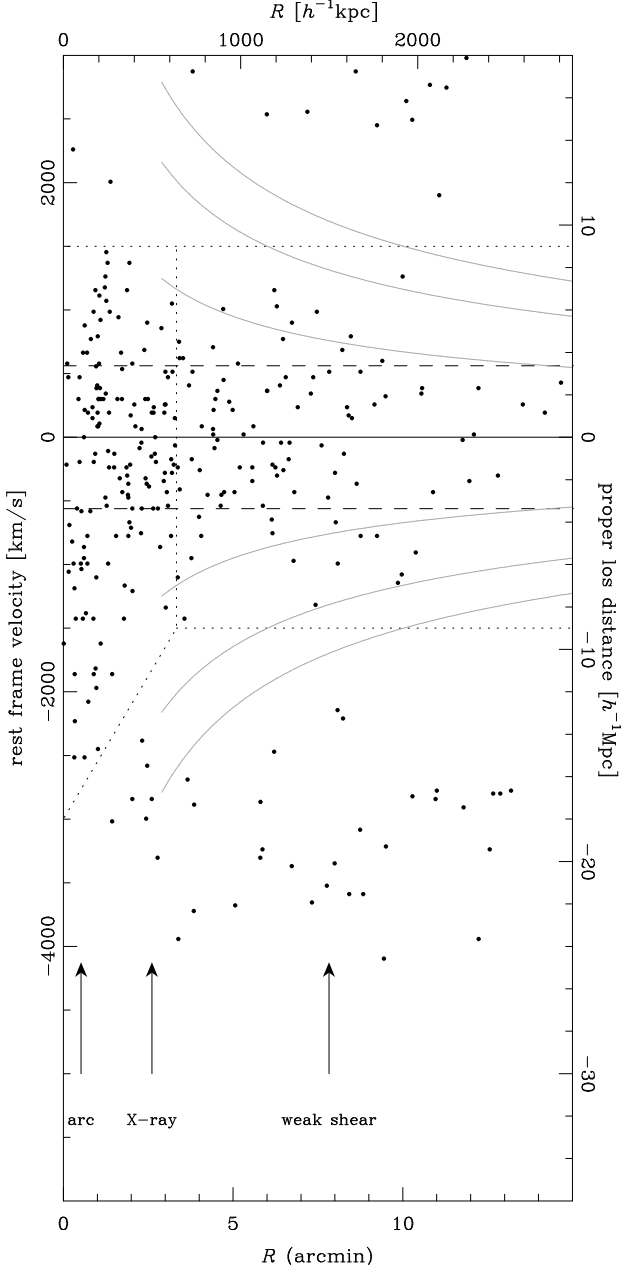


**Fig. 2.** Redshift  $z$  plotted against angular distance  $R$  from the projected cluster centre for the galaxies around the cluster redshift. The left axis expresses redshift as relative velocity with respect to the mean redshift of component A (Eq. 1), the right axis as proper line-of-sight distance at the cluster redshift. Angular distance is converted to proper transverse distance on the top axis. The dashed horizontal lines indicate the velocity dispersion of component A (Eq. 2), the dotted lines denote limits for the samples used in Sect. 2.2. The solid curves mark the escape velocities for masses inside radius  $R$  of  $1$ ,  $3$  and  $5 \times 10^{14} M_{\odot}$ . Arrows mark the position of the giant arc and the X-ray and weak shear detection limits.

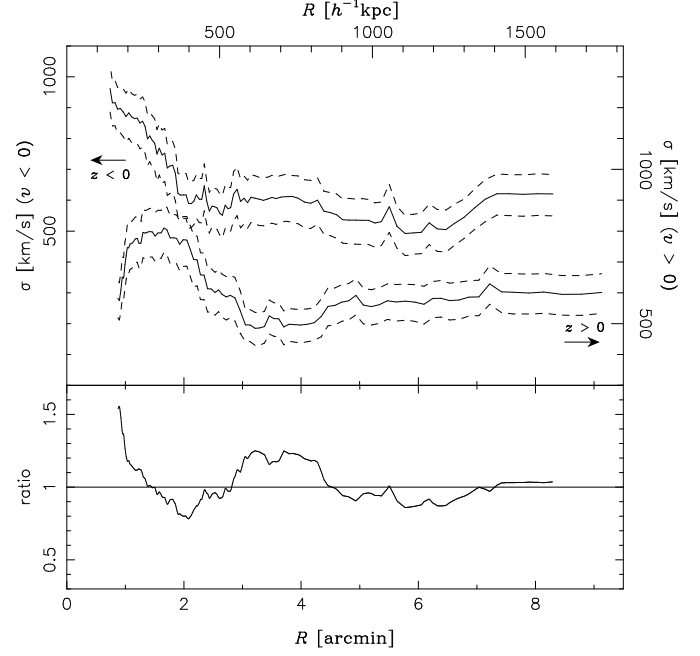


**Fig. 3.** Velocity dispersion profiles for galaxies with negative and positive velocity with respect to the mean redshift of cluster component A, which was held fixed at  $z_A = 0.3946$ . The profiles were computed using sliding averages in bins containing 30 galaxies. The error bands give  $1\sigma$  errors determined from bootstrap resampling (10000 realisations). The curve for positive velocities was shifted by  $300 \text{ km s}^{-1}$  for clarity, with the corresponding velocity values marked on the right-hand axis. The bottom panel shows the ratio of the dispersions for galaxies with negative and positive velocities.

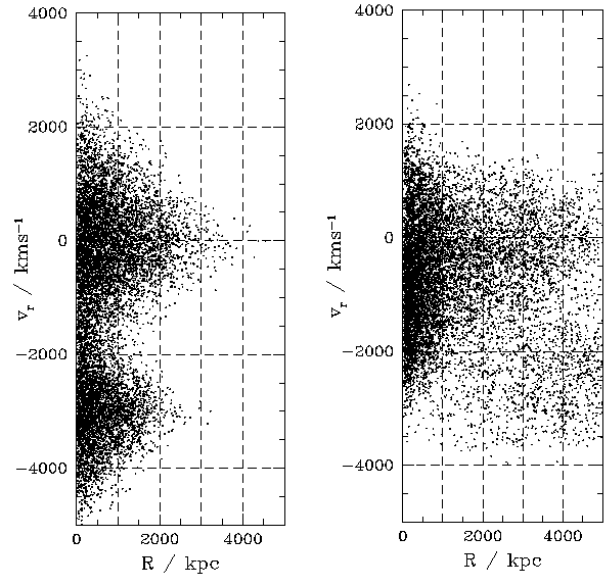


**Fig. 7.** The “observed” redshift distribution of particles in the collision between the simulated clusters. The left panel shows the initial conditions whilst the right panel shows the data 3 Gyrs after the collision. This is to be compared with Fig. 2.

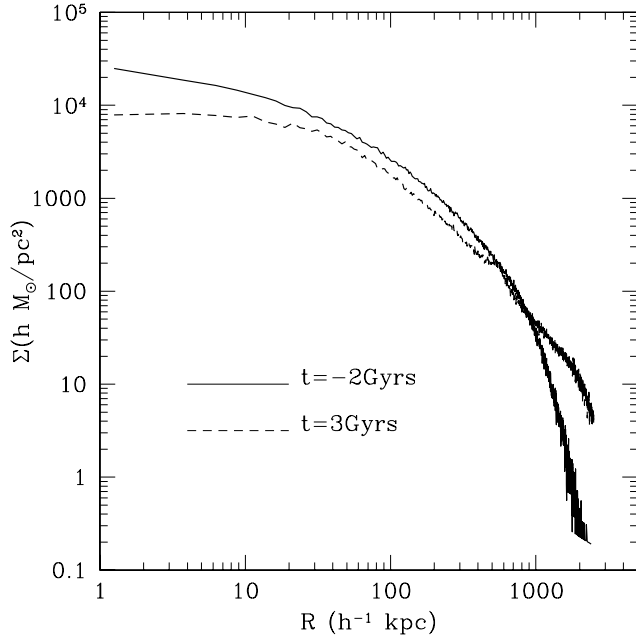


**Fig. 8.** The surface mass density profiles projected along the merger axis before (solid curve) and after the collision (dashed curve). The central surface mass density after the collision is very close to that measured by Tyson et al. (1998).

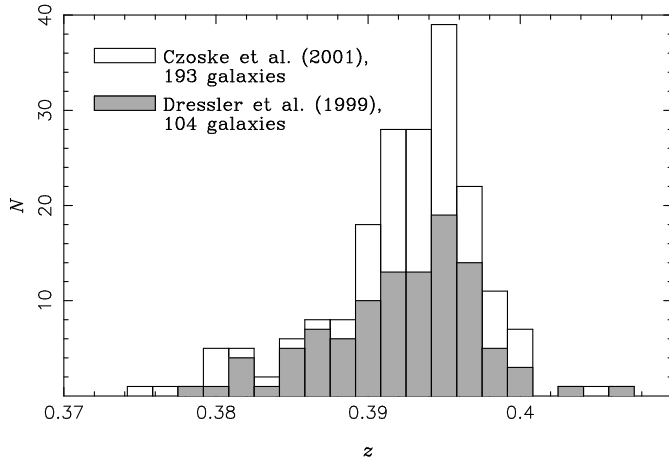


**Fig. 9.** Comparison of redshift histograms of the data of D99 (corrected for the misidentifications discussed in Paper I) and Paper I (these include the data of D99), constrained to the area covered by D99, clustercentric distance  $< 5'$ . Bin widths and centres are the same as in the inset of Figure 2 of D99.

This figure "Figure6.jpg" is available in "jpg" format from:

<http://arxiv.org/ps/astro-ph/0111118v1>